Chinese Chemical Letters 37 (2026) 110827

Contents lists available at ScienceDirect

Chinese Chemical Letters

journal homepage: www.elsevier.com/locate/cclet

Rational synthesis of highly charged E_9 (E = Ge, Sn) dimer and trimer with Nb/Au bridges

Ya-Shan Huang[a], Wen-Juan Tian[b,*], Jing-Xuan Zhang[c,*], Zhong-Ming Sun[a,*]

[a] State Key Laboratory of Elemento-Organic Chemistry, Tianjin Key Lab of Rare Earth Materials and Applications, School of Materials Science and Engineering, Nankai University, Tianjin 300350, China
[b] Institute of Molecular Science, Shanxi University, Taiyuan 030006, China
[c] Department of Chemistry, The Hong Kong University of Science and Technology, Clear Water Bay, Kowloon, Hong Kong 999077, China

ARTICLE INFO

Article history:
Received 26 November 2024
Revised 24 December 2024
Accepted 6 January 2025
Available online 9 January 2025

Keywords:
Oxidation-coupled clusters
Germanium cluster
Tin cluster
FAMO analysis
PIO analysis

ABSTRACT

Oxidation-coupled clusters of $[E_9]^{4-}$ are rarely synthesised, and the investigation of their reactivity is profoundly hindered by their high charge and limited yield. In this study, we successfully synthesized two Nb-containing clusters $[(Ge_9\text{–}Ge_9)(NbCp_2)_2]^{4-}$ (**1a**) and $[(Ge_9{=}Ge_9{=}Ge_9)NbCp_2]^{5-}$ (**2a**), by reacting $[Ge_9\text{–}Ge_9]^{6-}$ and $[Ge_9{=}Ge_9{=}Ge_9]^{6-}$ with $NbCp_4$. Theoretical calculations indicate that the formation of **1a** and **2a** from dimer and trimer is thermodynamically favorable. Furthermore, a Au-containing cluster incorporating the dimeric $[Sn_9\text{–}Sn_9]^{6-}$ cluster, $[Au(Sn_9\text{–}Sn_9)]^{5-}$ (**3a**), was successfully synthesized, despite the inability to independently synthesize $[Sn_9\text{–}Sn_9]^{6-}$. A systematic bonding analysis was conducted on these newly synthesized clusters and their parent structures to investigate their bonding patterns.

© 2026 Published by Elsevier B.V. on behalf of Chinese Chemical Society and Institute of Materia Medica, Chinese Academy of Medical Sciences.

The variability in size, shape, and composition leads to non-monotonic and unpredictable changes in cluster properties, creating opportunities for the development of new materials with tailored properties, which are extensively utilized in nanoscience and nanotechnology [1,2]. Although group 14 clusters have been widely studied in recent years, research into anionic clusters has primarily been focused on the reactivity of $[E_9]^{4-}$ (E = Si, Ge, Sn, Pb) [3–5]. Experiments have revealed the structural and electronic flexibility of $[E_9]^{4-}$, enabling their reactions with multiple organometallic compounds, while the limited availability of starting materials has hampered the synthesis of novel clusters, particularly large clusters comprising 18 or more atoms [6–19]. Most large clusters are formed by the fusion of several smaller building clusters [20–31], with only a few arising from the oxidative coupling of monomers, including $[Ge_9\text{–}Ge_9]^{6-}$ (Fig. 1a) [32], $[Ge_9{=}Ge_9{=}Ge_9]^{6-}$ (Fig. 1b) [33], $[E_9{=}E_9{=}E_9{=}E_9]^{8-}$ (E=Ge, Sn, Fig. 1c) [34,35], and infinite chains $^1_\infty[-(Ge_9^{2-})-]$ (Fig. 1d) [36]. The high charge of these oxidative-coupled clusters, along with their limited yield, impedes the exploration of their reactivity. Several functionalized clusters containing the $[Ge_9\text{–}Ge_9]$ unit have been reported, such as $[^tBu\text{–}Ge_9\text{–}Ge_9\text{–}^tBu]^{4-}$ [37], $[Ph_2Sb\text{–}Ge_9\text{–}Ge_9\text{–}SbPh_2]^{4-}$ [38], and $[R_3E\text{–}Ge_9\text{–}Ge_9\text{–}ER_3]^{4-}$ (E = Ge, Sn; R = Me, pH) [39]. Albeit experimental and theoretical calculations suggest that such germanium clusters likely result from the dimerization of monosubstituted monomers, their successful synthesis hints at the potential of oxidation-coupled germanium clusters as precursors for reacting with organometallic compounds. For Sn, although the stable $[Sn_9]^{3-}$ cluster has been reported, many attempts to synthesize $[Sn_9\text{–}Sn_9]^{6-}$, analogous to $[Ge_9\text{–}Ge_9]^{6-}$, have been unsuccessful. To date, only one cluster containing $[Sn_9\text{–}Sn_9]^{6-}$ unit has been synthesized, namely $[Ag(Sn_9\text{–}Sn_9)]^{5-}$, in which the dimeric $[Sn_9\text{–}Sn_9]^{6-}$ is coordinated with an Ag^+ ion (Fig. 1e) [40]. This prompted us to explore the oxidation-coupled clusters of $[Sn_9]^{4-}$. Here in, we investigated the reactivity of $[Ge_9\text{–}Ge_9]^{6-}$ and $[Ge_9{=}Ge_9{=}Ge_9]^{6-}$ with $NbCp_4$, leading to the formation of two Nb-containing compounds $[K(2.2.2\text{-crypt})]_4[(Ge_9\text{–}Ge_9)(NbCp_2)_2]\cdot en$ (**1**) and $[K(2.2.2\text{-crypt})]_5[(Ge_9{=}Ge_9{=}Ge_9)NbCp_2]\cdot en$ (**2**). The synthesis of compounds **1** and **2** not only initiates exploration into the reactivity of highly charged clusters $[Ge_9\text{–}Ge_9]^{6-}$ and $[Ge_9{=}Ge_9{=}Ge_9]^{6-}$ but also lays a foundation for rationalizing the synthesis of larger species. Moreover, a Au-containing compound $[K(2.2.2\text{-crypt})]_5[AuSn_{18}]\cdot en\cdot tol$ (**3**), isostructural with $[Ag(Sn_9\text{–}Sn_9)]^{5-}$, has also been synthesized and characterized. ESI-MS analysis and theoretical calculations suggest that the $[Sn_9\text{–}Sn_9]^{6-}$ has low stability, and the $[Au]^+$ center in **3a** play an important role in stabilizing the $[Sn_9\text{–}Sn_9]^{6-}$ kernel. This could explain why $[Sn_9\text{–}Sn_9]^{6-}$ has not been successfully synthesized thus far. The successful synthesis of this gold compound enhances the understanding of oxidation-coupled clusters of $[Sn_9]^{4-}$.

* Corresponding authors.
E-mail addresses: tianwenjuan@sxu.edu.cn (W.-J. Tian), jzhangbm@connect.ust.hk (J.-X. Zhang), sunlab@nankai.edu.cn (Z.-M. Sun).

https://doi.org/10.1016/j.cclet.2025.110827
1001-8417/© 2026 Published by Elsevier B.V. on behalf of Chinese Chemical Society and Institute of Materia Medica, Chinese Academy of Medical Sciences.

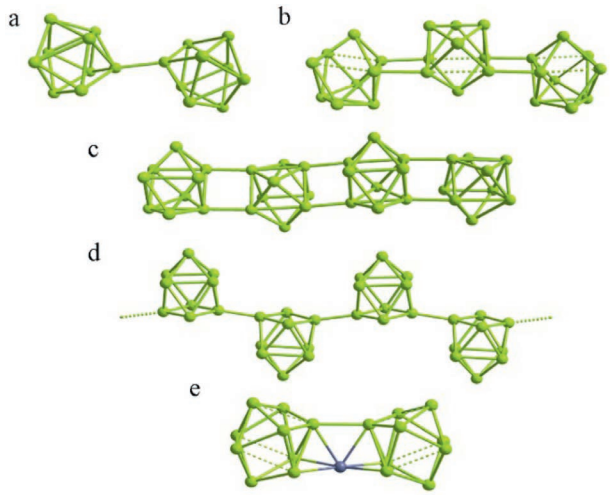


Fig. 1. Structures of the oxidative-coupled clusters. (a) $[Ge_9–Ge_9]^{6-}$, (b) $[Ge_9=Ge_9=Ge_9]^{6-}$, (c) $[E_9=E_9=E_9=E_9]^{8-}$ (E = Ge, Sn), (d) $^{1}_{\infty}[-(Ge_9^{2-})-]$, (e) $[Ag(Sn_9–Sn_9)]^{5-}$.

The previously reported synthetic methods for $[Ge_9–Ge_9]^{6-}$ and $[Ge_9=Ge_9=Ge_9]^{6-}$ face constraints related to composition, yield, and solvent, which complicate subsequent reactions. To address this, we sought to find an efficient method for synthesizing large quantities of $[Ge_9–Ge_9]^{6-}$ and $[Ge_9=Ge_9=Ge_9]^{6-}$ in solution and to explore their reactivity through *in-situ* reactions in solution. After many attempts, we discovered that the Nb(IV) complex, $NbCp_4$, functions as a mild oxidizing agent for the formation of $[Ge_9–Ge_9]^{6-}$ and $[Ge_9=Ge_9=Ge_9]^{6-}$. Similar oxidation reactions have been noted in previous cluster formations, such as $Ge_{18}[Si(SiMe_3)_3]_6$ and Ge_{24}^{4-}, where Fe(II) and Co(II) salts act as oxidizing agents, respectively [22,41]. ESI-MS analysis of the reaction solution containing K_4Ge_9, a small quantity of $NbCp_4$ and 2.2.2-crypt (Fig. S8 in Supporting information) indicated the presence of significant amounts of $\{[K(2.2.2\text{-crypt})][Ge_{18}]\}^-$ (Fig. S9 in Supporting information), $\{[K(2.2.2\text{-crypt})]_3[Ge_{18}]\}^-$ (Fig. S10 in Supporting information), and $\{[K(2.2.2\text{-crypt})]_3[Ge_{27}]\}^-$ (Fig. S11 in Supporting information), enabling us to explore the reactivity of $[Ge_9–Ge_9]^{6-}$ and $[Ge_9=Ge_9=Ge_9]^{6-}$. Reaction of K_4Ge_9 with excess $NbCp_4$ in the presence of 2.2.2-crypt at room temperature yields the dimeric derivative **1**. Elevating the reaction temperature to 70 °C and prolonging the reaction time yields the trimeric derivative **2**. Furthermore, according to the given reaction energies, it is thermodynamically advantageous to form **1** and **2** (Eqs. 1 and 2). We also explored the oxidative coupling of $[Sn_9]^{4-}$ to form $[Sn_9–Sn_9]^{6-}$, however, this attempt was unsuccessful. Given that the only known dimeric Sn_9 cluster is the Ag-containing compound, we tried reacting K_4Sn_9 with the heavier analog, $Au(PPh_3)Me$, and successfully synthesized compound **3**. Detailed experimental procedures are provided in Supporting information.

$$Ge_{18}^{6-} + 2Nb(Cp)_2^{+} \rightarrow Ge_{18}(NbCp_2)_2^{4-} \quad \Delta E = -168.76\ \text{kcal/mol} \quad (1)$$

$$Ge_{27}^{6-} + Nb(Cp)_2^{+} \rightarrow Ge_{27}Nb(Cp)_2^{5-} \quad \Delta E = -80.64\ \text{kcal/mol} \quad (2)$$

Crystals of **1**–**3** were characterized by single-crystal X-ray diffraction analysis. Compound **1** crystallizes in the orthorhombic space group *Pbcn* and the asymmetric unit contains one cluster anion $[(Ge_9–Ge_9)(NbCp_2)_2]^{4-}$, two $[K(2.2.2\text{-crypt})]^+$ cations, and one en molecule (Fig. S2 in Supporting information). The cluster anion exhibits statistical disorder on the atomic level, manifesting a major orientation (67 % occupancy) along with a minor contributor, and thus subsequent discussions of the structure will primarily focus on the former. In cluster **1a**, the configuration of the two $[Ge_9]$ units maintains a monocapped square antiprism, akin to the structure observed in the related $[Ge_9–Ge_9]^{6-}$. Conventionally, the two $[Ge_9]$ cages within the $[Ge_9–Ge_9]^{6-}$ dimer exhibit a *transoid* arrangement. However, upon the incorporation of two $[NbCp_2]^+$fragments, the two nine-atom cages in **1a** show a sterically less favorable *cisoid* conformation (Fig. 2a). This phenomenon, characterized by a crowded *cisoid* conformation, is also evident in $[[Ag(Sn_9–Sn_9)]^{5-}$ and $[(Ge_9)_2In(C_6H_5)]^{4-}$ [40,42]. The bond distance between the two $[Ge_9]$ cages in **1a** measures 2.443 Å, comparable to the inter-cluster bond distance of 2.488 Å in $[Ge_9–Ge_9]^{6-}$, shorter than that observed in $[(Ge_9)_2In(C_6H_5)]^{4-}$ (2.583 Å), indicating a two-center, two-electron localized bond. Furthermore, the two $[NbCp_2]$ fragments coordinate with the Ge atoms situated on the capped squares within the Ge_9 cages (Ge4, Ge5, Ge4′, and Ge5′, respectively), forming four Nb–Ge bonds with an average length of 2.730 Å. These contacts are comparable to those in $[(\eta^6\text{-}C_6H_3Me_3)\text{-}NbHGe_6]^{2-}$ (2.749 Å) [9] and $Nb(\eta^5\text{-}C_5H_4SiMe_3)_2(H)_2(GePh_3)$ (2.710 Å) [43], shorter than those in $[Nb@Ge_{13}]^{3-}$ (2.817 Å) [44], $[Nb@Ge_{14}]^{3-}$ (2.869 Å) [44] and $[Nb@Ge_8As_6]^{3-}$ (2.965 Å) [45], but longer than those in $Cp_2NbH(GeMe_3)_2$ (2.660 Å) [46] and $[(\eta^6\text{-}C_6H_3Me_3)NbGe_6Nb(\eta^6\text{-}C_6H_3Me_3)]^{2-}$ (2.615 Å) [9]. The Nb–C bond distances (2.379 Å, ave.) are statistically indistinguishable from those observed in the parent compound $NbCp_4$ (2.387 Å) [47]. The average Ge–Ge distances around the capping atom (d_{cap}), at the capped square (d_{csq}), at the waist (d_{wst}), at the open square (d_{osq}) are similar to those in $[Ge_9–Ge_9]^{6-}$: d_{cap} = 2.579 Å (**1a**), 2.578 Å ($[Ge_9–Ge_9]^{6-}$); d_{csq} = 2.763 Å (**1a**), 2.810 Å ($[Ge_9–Ge_9]^{6-}$); d_{wst} = 2.628 Å (**1a**), 2.604 Å ($[Ge_9–Ge_9]^{6-}$); d_{osq} = 2.573 Å (**1a**), 2.580 Å ($[Ge_9–Ge_9]^{6-}$). Thus, **1a** can be formally rationalized as a $[Ge_9–Ge_9]^{6-}$ dimer coordinating to two $[NbCp_2]^+$ with formal Nb^{3+} cation.

Compound **2** crystallizes in the monoclinic space group $P2_1/c$, with the asymmetric unit containing one $[(Ge_9=Ge_9=Ge_9)NbCp_2]^{5-}$ anion, five $[K(2.2.2\text{-crypt})]^+$ cations, and one en molecule (Fig. S4 in Supporting information). As observed in $[Ge_9=Ge_9=Ge_9]^{6-}$, each of the three $[Ge_9]$ cages in **2a** adopts a tricapped trigonal prisms configuration, elongated along two prismatic edges (Ge2–Ge5, Ge3–Ge4, Ge11–Ge12, Ge13–Ge14, Ge20–Ge23, Ge21–Ge22, Fig. 2b). These cages are interconnected by two exo-bonds along the elongated prismatic edges. Notably, the Ge–Ge bond distances in **2a** closely resemble those observed in $[Ge_9=Ge_9=Ge_9]^{6-}$. However, the incorporation of the $[NbCp_2]^+$ fragment induces a deviation from linearity in $[Ge_9=Ge_9=Ge_9]^{6-}$, causing it to tilt towards the $[NbCp_2]$ moiety. This tilt is accompanied by the formation of two Nb–Ge bonds, with lengths of 2.711 Å and 2.653 Å. The angle between the two Nb–Ge bonds (∠Ge17–Nb–Ge19) measures 83.009°, similar to the corresponding angles observed in **1a** (∠Ge4–Nb1–Ge5′ = ∠Ge4′–Nb1′–Ge5 = 82.189°). Similarly, **2a** can also be rationalized as one $[NbCp_2]^+$ fragment with formal Nb^{3+}cation, along with a $[Ge_9=Ge_9=Ge_9]^{6-}$ trimer. The long axes of **1a** and **2a** measure 9.003 Å (Fig. 2c) and 14.591 Å (Fig. 2d), respectively, which are slightly shorter than those in $[Ge_9–Ge_9]^{6-}$ (9.266 Å) and $[Ge_9=Ge_9=Ge_9]^{6-}$ (14.241 Å).

Compound **3** crystallizes in the triclinic space group *P*-1, with the asymmetric unit containing one cluster anion $[Au(Sn_9–Sn_9)]^{5-}$, five $[K(2.2.2\text{-crypt})]^+$ cations, one en molecule, and one toluene molecule (Fig. S6 in Supporting information). The structure of **3a** is isostructural with the previously reported cluster $[Ag(Sn_9–Sn_9)]^{5-}$. The Au^+ ion is positioned between two $[Sn_9]$ cages, each adopting a tricapped trigonal prismatic configuration, and is coordinated to the Sn atoms on the triangular faces of both $[Sn_9]$ cages, forming six Au-Sn bonds (Fig. 3a). Notably, the Au^+ ion and four coordinated Sn atoms (Sn4, Sn5, Sn11, Sn12) are nearly coplanar,

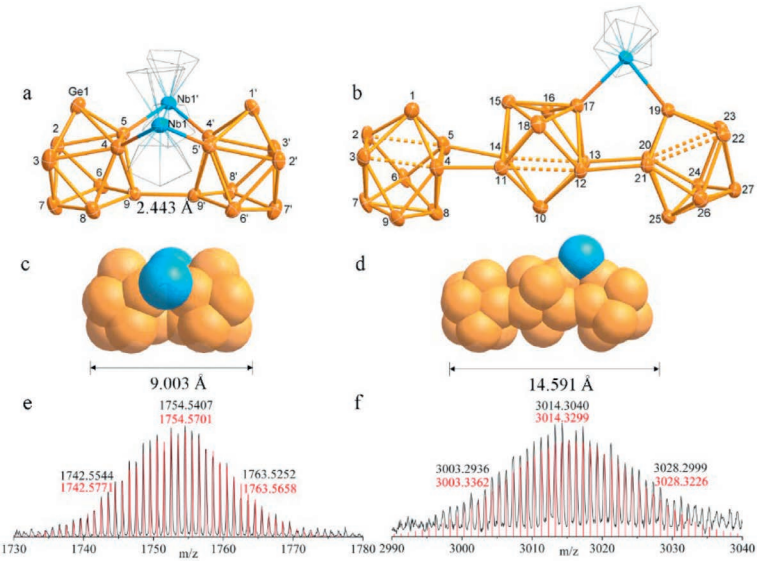


Fig. 2. ORTEP representation of the cluster anion (a) $[(Ge_9–Ge_9)(NbCp_2)_2]^{4–}$ and (b) $[(Ge_9=Ge_9=Ge_9)NbCp_2]^{5–}$ (thermal ellipsoids are drawn at 50% probability). Space-filling representation of (c) $[(Ge_9–Ge_9)(NbCp_2)_2]^{4–}$ and (d) $[(Ge_9=Ge_9=Ge_9)NbCp_2]^{5–}$. Negative ion ESI mass peaks corresponding to (e) $\{[Ge_{18}Nb_2Cp_4]\}^–$ and (f) $\{[K(2.2.2\text{-crypt})]_2[Ge_{27}NbCp_2]\}^–$. The experimental mass distributions are shown in black, and the theoretical masses of the isotope distributions are depicted in red.

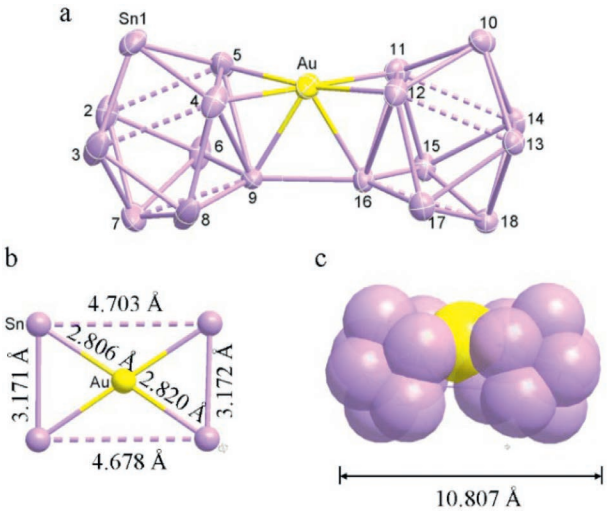


Fig. 3. (a) ORTEP representation of the cluster anion $[Au(Sn_9–Sn_9)]^{5–}$ (thermal ellipsoids are drawn at 50% probability). (b) The rectangle unit $[AuSn_4]$. (c) Space-filling representation of the crystal structure.

forming a rectangular arrangement (Fig. 3b). The four Au-Sn bonds within this rectangle (2.806–2.862 Å) are shorter than the other two (2.921 Å and 2.953 Å, respectively), but slightly longer than the sum of the covalent radii of Ge and Sn (2.75 Å) [48]. The long axis of the cage measures 10.807 Å (Fig. 3c), which is slightly shorter than that in $[Ag(Sn_9–Sn_9)]^{5–}$ (11.016 Å).

The presence of **1**–**3** was also confirmed through energy dispersive X-ray spectrometry (EDX, Figs. S35-S37 in Supporting information) and ESI-MS (Figs. S12, S23, and S29 in Supporting information). ESI-MS analysis, conducted by dissolving crystals of compounds **1** and **2** in acetonitrile (ACN) solution, reveals mass envelopes corresponding to the parent clusters, including $\{[Ge_{18}Nb_2Cp_4]\}^–$ (Fig. 2e), $\{[K(2.2.2\text{-crypt}]_2[Ge_{27}NbCp_2]\}^–$ (Fig. 2f), $\{[KGe_{27}NbCp_2]\}^{2–}$ (Fig. S24 in Supporting information), $\{[K(2.2.2\text{-crypt}][Ge_{27}NbCp_2]\}^{2–}$ (Fig. S26 in Supporting information). Furthermore, inevitable decomposition processes in solution lead to the formation of a series of fragments (Figs. S13-S21, S25, and S27 in Supporting information). The ESI-MS of compound **3** shows fragments derived from the parent compound, including $\{[AuSn_9]\}^–$ (Fig. S31 in Supporting information), and $\{[K(2.2.2\text{-crypt})][Sn_9]\}^–$ (Fig. S33 in Supporting information). This suggests the lower stability of $[Sn_9–Sn_9]$, which may explain why $[Sn_9–Sn_9]^{6–}$ has not been successfully synthesized thus far.

Theoretical calculations have been performed to understand the electronic structures of the synthesized species. To deal with the inter-fragment interactions among multiple $[E_9]$ units and metal centers, fragment aligned molecular orbital (FAMO) analysis has been performed to give a fragment-based description of the electronic structures of relevant clusters.

In the case of $[Ge_{18}(NbCp_2)_2]^{4–}$, FAMO analysis is performed with two $[Ge_9]^{2–}$ moieties and two $[NbCp_2]^+$ moieties as the reference fragments. The occupied orbitals of the reference fragments are found to be relatively inactive (FAMO eigenvalues all beyond 0.92), which means these orbitals do not deform much compared to their shapes in isolated fragments (Fig. 4a). In addition, because the total charge is not conserved during fragmentation, there exists one orbital that is occupied in the whole cluster but not in isolated fragments (Fig. 4a). By comparing it against the frontier orbitals of a single $[Ge_9]^{2–}$ fragment, one can see that this orbital largely resembles the in-phase combination of the LUMOs of two $[Ge_9]^{2–}$ fragments, or equivalently, the SOMOs of $[Ge_9]^{3–}$ fragments. This implies that the additional two electrons in $[Ge_{18}(NbCp_2)_2]^{4–}$ reside in a bonding orbital between two cages forming a single bond. This is consistent with the usual understanding of the inter-cage single bond in $[Ge_9–Ge_9]^{6–}$ cluster, except that this bond is not completely localized at the two bonded atoms, but in fact delocalized over the whole cage. The $[NbCp_2]^+$ fragments do not significantly participate in this inter-cage bonding, but serve as a glue that bridges the two cages by dative interactions as demonstrated. Such interaction can be revealed by the deformation of the matched FAMOs (Fig. 4a), or the principal interacting orbital (PIO) analysis between $[Ge_9–Ge_9]^{6–}$ and $[(NbCp_2)_2]^{2+}$ fragments (Figs. S38-S41 in Supporting information), which shows dative interactions from the cage to the Nb 4d and 5s orbitals [49]. The Nb center of each $[NbCp_2]^+$ moiety has 14 valence electrons in total, leaving two orbitals available for bonding with the Ge cages, thus there are four dative bonds from $[Ge_9–Ge_9]^{6–}$ to $[(NbCp_2)_2]^{2+}$ in total, which are exactly the top four PIOs. The overall bonding

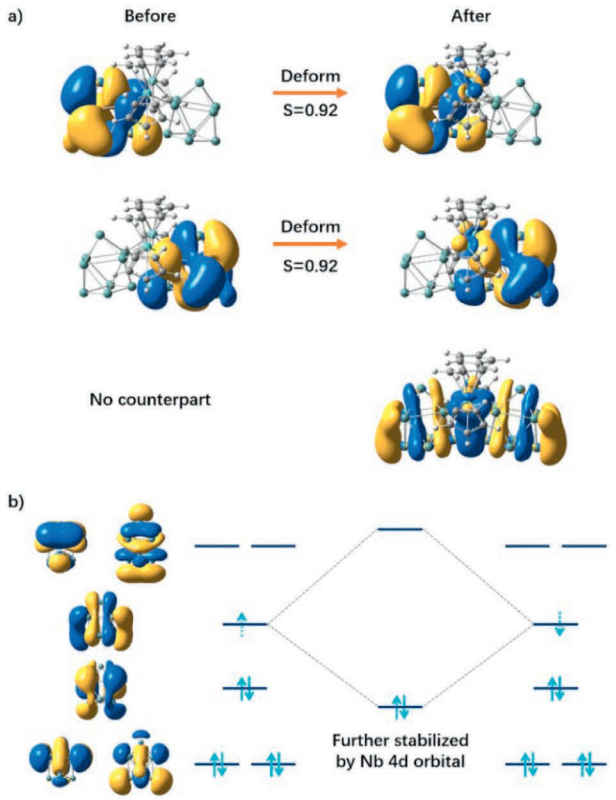


Fig. 4. FAMO analysis on the $[Ge_{18}(NbCp_2)_2]^{4-}$ cluster with respect to two $[Ge_9]^{2-}$ fragments and two $[NbCp_2]^{+}$ fragments. (a) Three frontier FAMO pairs are shown here including one unmatched FAMO and two matched FAMOs with least overlaps. (b) Illustrative orbital diagram showing the interaction betwee the two $[Ge_9]$ fragments. Note the close resemblance between the unmatched FAMO in (a) and the LUMO of $[Ge_9]^{2-}$ in (b).

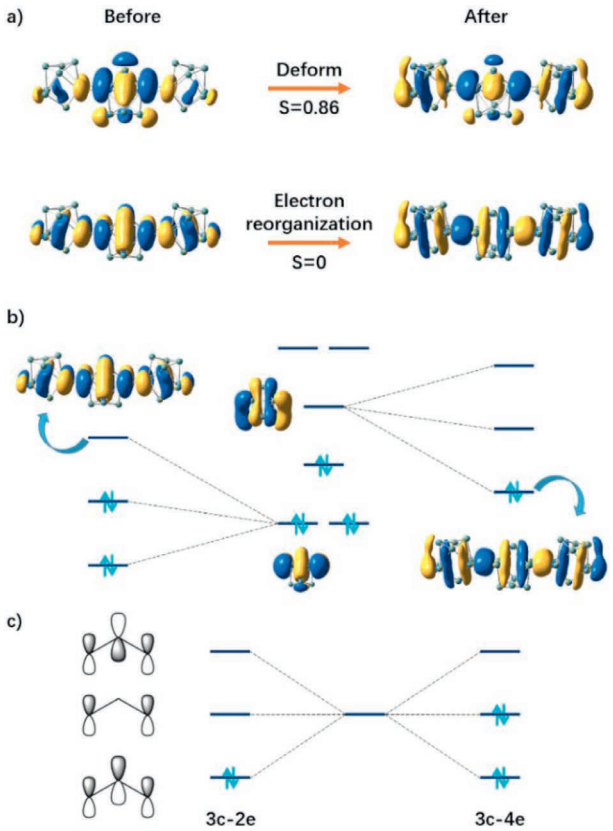


Fig. 5. (a) FAMO analysis on the $[Ge_9{=}Ge_9{=}Ge_9]^{6-}$ cluster with respect to three $[Ge_9]^{2-}$ fragments. (b) Illustrative orbital diagram showing the interaction among three $[Ge_9]$ fragments when affording $[Ge_9{=}Ge_9{=}Ge_9]^{6-}$ cluster. (c) Illustrative orbital diagram of propenyl for comparison.

pattern can be described by an orbital interaction diagram as shown in Fig. 4b.

The electronic structure of compound **2** is relatively more complicated. To clearly describe its bonding pattern, two rounds of FAMO analysis have been performed. The first round of FAMO analysis was performed on $[Ge_{27}NbCp_2]^{5-}$ with respect to $[Ge_{27}]^{6-}$ and $[NbCp_2]^{+}$ moieties, in which no significant orbital deformation was observed (FAMO eigenvalues all beyond 0.96), showing that the interaction between $[Ge_9{=}Ge_9{=}Ge_9]^{6-}$ and $[NbCp_2]^{+}$ moieties is simply donor-accpetor interaction as in $[Ge_{18}(NbCp_2)_2]^{4-}$ (Fig. S38 in Supporting information). This is also in line with the PIO analysis results with the same fragmentation (Figs. S42-S44 in Supporting information). However, a second round of FAMO analysis on $[Ge_9{=}Ge_9{=}Ge_9]^{6-}$ with respect to three $[Ge_9]^{2-}$ fragments shows significant electron reorganization. There exists an orbital which is occupied in the cluster but unoccupied in the isolated fragments, and another orbital which is unoccupied in the cluster but occupied in the isolated fragments (Fig. 5a). This means electron reorganization occurs when these three fragments form a $[Ge_9{=}Ge_9{=}Ge_9]^{6-}$ cluster. Close examination reveals that the unmatched FAMO pair are nothing but an all-in-phase combination of the LUMO of the $[Ge_9]^{2-}$ moieties, and an all-out-of-phase combination of the HOMO-1 of the $[Ge_9]^{2-}$ moieties. In other words, the three $[Ge_9]^{2-}$ moieties are connected through two delocalized bonds, one 3c-2e bond and one 3c-4e bond. An illustrative orbital interaction diagram is shown in Fig. 5b to describe the electronic structure of $[Ge_9{=}Ge_9{=}Ge_9]^{6-}$. This is in analogy with the delocalized bonding in propene cation and anion (Fig. 5c), except that each center is now a cage not an atom. Besides, the fact that each cage contributes two orbitals involved in the delocalized bonding is also reflected by the PIO analysis on this compound with one $[Ge_9]$ cage as a fragment and the rest of atoms as the other in which the top two PIOs exactly bare the shape of the LUMO and HOMO-1 of a $[Ge_9]^{2-}$ cluster (Fig. S43). Such bonding scheme explains that why three $[Ge_9]^{2-}$ moieties can be linked together without additional electrons when affording the $[Ge_9{=}Ge_9{=}Ge_9]^{6-}$ cluster, while two $[Ge_9]^{2-}$ fragments need two more electrons to afford the $[Ge_9{-}Ge_9]^{6-}$ cluster.

The electronic structure of compound $[AuSn_{18}]^{5-}$ is somehow similar to that of $[Ge_{18}(NbCp_2)_2]^{4-}$. Two electrons enter the in-phase combination of the LUMOs of two $[Sn_9]^{2-}$ fragments, formally forming a single bond, to afford $[Sn_9{-}Sn_9]^{6-}$. However, FAMO analysis reveals that this bonding orbital between two cages has significant contributions from the $[Au]^{+}$ 6s orbital (Fig. 6). PIO analysis also suggests a prominent interaction between the Sn cage and the Au center (Fig. S45 in Supporting information). This hints the $[Au]^{+}$ center might play an important role in stabilizing the $[Sn_9{-}Sn_9]^{6-}$ kernel and might explain why bare $[Sn_9{-}Sn_9]^{6-}$ cluster has never been isolated.

In summary, we have established that the $[Ge_9{-}Ge_9]^{6-}$ and $[Ge_9{=}Ge_9{=}Ge_9]^{6-}$ present in the reaction solution can be used as starting materials to react with organometallic compounds to form larger clusters. Their reactions with $NbCp_4$ yield two Nb-containing clusters $[(Ge_9{-}Ge_9)(NbCp_2)_2]^{4-}$ and $[(Ge_9{=}Ge_9{=}Ge_9)NbCp_2]^{5-}$. In addition, a Au-containing cluster incorporating a dimeric $[Sn_9{-}Sn_9]^{6-}$ unit has also been characterized. FAMO and PIO analysis indicate that the interaction between Ge cage and $[NbCp_2]^{+}$ moieties are predominantly donor-acceptor interaction, while inter-cage bonding is also investigated and discussed. The strategy in our work provides new starting materials for reasonable synthe-

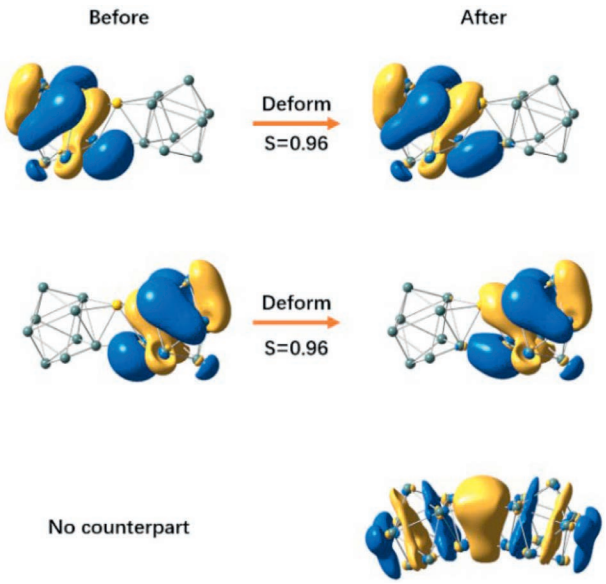


Fig. 6. FAMO analysis on the $[AuSn_{18}]^{5-}$ cluster with respect two $[Sn_9]^{2-}$ fragments and a $[Au]^{+}$ fragment.

sis of large clusters, opening up new opportunities for applications in nanoscience and nanotechnology.

Declaration of competing interest

The authors declare that they have no known competing financial interests or personal relationships that could have appeared to influence the work reported in this paper.

CRediT authorship contribution statement

Ya-Shan Huang: Writing – review & editing, Writing – original draft, Methodology, Investigation, Formal analysis, Data curation. **Wen-Juan Tian:** Writing – review & editing, Writing – original draft, Investigation, Formal analysis, Data curation. **Jing-Xuan Zhang:** Writing – review & editing, Writing – original draft, Investigation, Formal analysis, Data curation. **Zhong-Ming Sun:** Writing – review & editing, Writing – original draft, Supervision, Project administration, Funding acquisition, Conceptualization.

Acknowledgments

This work was supported by the National Natural Science Foundation of China (Nos. 22425107 (Z.-M. Sun), 92461303 (Z.-M. Sun), 22371140 (Z.-M. Sun), 92161102 (Z.-M. Sun), and 22402108 (W.-J. Tian)).

Supplementary materials

Supplementary material associated with this article can be found, in the online version, at doi:10.1016/j.cclet.2025.110827.

References

[1] J. Zhao, Q. Du, S. Zhou, V. Kumar, Chem. Rev. 120 (2020) 9021–9163.
[2] P. Jena, Q. Sun, Chem. Rev. 118 (2018) 5755–5870.
[3] R.J. Wilson, N. Lichtenberger, B. Weinert, S. Dehnen, Chem. Rev. 119 (2019) 8506–8554.
[4] C. Liu, Z.M. Sun, Coordin. Chem. Rev. 382 (2019) 32–56.
[5] T.F. Fässler, Coordin. Chem. Rev. 215 (2001) 347–377.
[6] J.Q. Wang, S. Stegmaier, T.F. Fässler, Angew. Chem. Int. Ed. 121 (2009) 2032–2036.
[7] B. Zhou, M.S. Denning, D.L. Kays, J.M. Goicoechea, J. Am. Chem. Soc. 131 (2009) 2802–2803.
[8] M.W. Hull, S.C. Sevov, Angew. Chem. Int. Ed. 46 (2007) 6695–6698.
[9] A.M. Li, Y. Wang, P.Y. Zavalij, et al., Inorg. Chem. 60 (2021) 14697–14705.
[10] G. Espinoza-Quintero, J.C.A. Duckworth, W.K. Myers, J.E. McGrady, J.M. Goicoechea, J. Am. Chem. Soc. 136 (2014) 1210–1213.
[11] J. Campbell, H.P.A. Mercier, H. Franke, et al., Inorg. Chem. 41 (2002) 86–107.
[12] H.L. Xu, L. Q, Z.M. Sun, Chin. J. Chem. 41 (2023) 2432–2438.
[13] D.O. Downing, P. Zavalij, B.W. Eichhorn, Eur. J. Inorg. Chem. 2010 (2010) 890–894.
[14] Y.S. Huang, D. Chen, J. Zhu, Z.M. Sun, Chin. Chem. Lett. 33 (2022) 2139–2142.
[15] B. Kesanli, J. Fettinger, B. Eichhorn, Angew. Chem. Int. Ed. 40 (2001) 2300–2302.
[16] B.J.L. Witzel, W. Klein, J.V. Dums, M. Boyko, T.F. Fässler, Angew. Chem. Int. Ed. 58 (2019) 12908–12913.
[17] B. Zhou, T. Krämer, A.L. Thompson, J.E. McGrady, J.M. Goicoechea, Inorg. Chem. 50 (2011) 8028–8037.
[18] E.N. Esenturk, J. Fettinger, B. Eichhorn, J. Am. Chem. Soc. 128 (2006) 9178–9186.
[19] A.M. Li, Y. Wang, P.Y. Zavalij, et al., Chem. Commun. 56 (2020) 10859–10862.
[20] J.M. Goicoechea, S.C. Sevov, J. Am. Chem. Soc. 127 (2005) 7676–7677.
[21] J.M. Goicoechea, S.C. Sevov, Angew. Chem. Int. Ed. 44 (2005) 4026–4028.
[22] H.L. Xu, N.V. Tkachenko, D.W. Szczepanik, et al., Nat. Commun. 13 (2022) 2149.
[23] A. Spiekermann, S.D. Hoffmann, F. Kraus, T.F. Fässler, Angew. Chem. Int. Ed. 46 (2007) 1638–1640.
[24] A. Spiekermann, S.D. Hoffmann, T.F. Fässler, I. Krossing, U. Preiss, Angew. Chem. Int. Ed. 46 (2007) 5310–5313.
[25] C. Liu, X. Jin, L.J. Li, et al., Chem. Sci. 10 (2019) 4394–4401.
[26] H.L. Xu, N.V. Tkachenko, Z.C. Wang, et al., Nat. Commun. 11 (2020) 5286.
[27] L. Qiao, C. Zhang, C.C. Shu, et al., J. Am. Chem. Soc. 142 (2020) 13288–13293.
[28] C.C. Shu, H.W.T. Morgan, L. Qiao, J.E. McGrady, Z.M. Sun, Nat. Commun. 11 (2020) 3477.
[29] H.W.T. Morgan, C.C. Shu, Z.M. Sun, J.E. McGrady, J. Am. Chem. Soc. 144 (2022) 8007–8017.
[30] Z.S. Li, W.X. Chen, H.W.T. Morgan, et al., Chem. Sci. 15 (2024) 1018–1026.
[31] W.X. Chen, Z.S. Li, H.W.T. Morgan, et al., Chem. Sci. 15 (2024) 4981–4988.
[32] L. Xu, S.C. Sevov, J. Am. Chem. Soc. 121 (1999) 9245–9246.
[33] A. Ugrinov, S.C. Sevov, J. Am. Chem. Soc. 124 (2002) 10990–10991.
[34] A. Ugrinov, S.C. Sevov, Inorg. Chem. 42 (2003) 5789–5791.
[35] N.V. Tkachenko, W.X. Chen, H.W.T. Morgan, et al., Chem. Commun. 58 (2022) 6223–6226.
[36] C. Downie, J.G. Mao, H. Parmer, A.M. Guloy, Inorg. Chem. 43 (2004) 1992–1997.
[37] M.W. Hull, A. Ugrinov, I. Petrov, S.C. Sevov, Inorg. Chem. 46 (2007) 2704–2708.
[38] A. Ugrinov, S.C. Sevov, J. Am. Chem. Soc. 125 (2003) 14059–14064.
[39] A. Ugrinov, S.C. Sevov, Chem. Eur. J. 10 (2004) 3727–3733.
[40] J.Q. Wang, B. Wahl, T.F. Fässler, Angew. Chem. Int. Ed. 49 (2010) 6592–6595.
[41] O. Kysliak, C. Schrenk, A. Schnepf, Angew. Chem. Int. Ed. 55 (2016) 3216–3219.
[42] D.F. Hansen, B. Zhou, J.M. Goicoechea, J. Organomet. Chem. 721-722 (2012) 53–61.
[43] A. Antinolo, F. Carrillo-Hermosilla, A. Castel, et al., Organometallics 17 (1998) 1523–1529.
[44] Y.S. Huang, Y. Xue, A. Muñoz-Castro, I.A. Popov, Z.M. Sun, Chem. Eur. J. 28 (2022) e202202192.
[45] S. Mitzinger, L. Broeckaert, W. Massa, F. Weigend, S. Dehnen, Chem. Commun. 51 (2015) 3866–3869.
[46] G.I. Nikonov, A.V. Churakov, M.Y. Antipin, Organometallics 22 (2003) 2178–2180.
[47] F. Calderazzo, C. Giardi, U. Englert, G. Pampaloni, J. Organomet. Chem. 630 (2001) 275–280.
[48] L. Pauling, J. Am. Chem. Soc. 69 (1947) 542–553.
[49] J.X. Zhang, F.K. Sheong, Z.Y. Lin, Chem. Eur. J. 24 (2018) 9639–9650.